Studies of Ligand Additions to Coordinatively Unsaturated Dirhenium Complexes Containing the Bulky PBu^t_3 Ligand

Richard D. Adams,* Burjor Captain, and Perry J. Pellechia

Department of Chemistry and Biochemistry, University of South Carolina, Columbia, South Carolina 29208

Received August 2, 2007

Five new complexes were obtained from the reaction of $Re_3(CO)_{12}(\mu\text{-}H)_3$ with PBu^t_3. These are $Re_2(CO)_8(\mu\text{-}PBu^t_2)(\mu\text{-}H)$, **1**, $Re_2(CO)_7(\mu\text{-}PBu^t_2)(PBu^t_2H)(\mu\text{-}H)$, **2**, $HRe(CO)_4(PBu^t_3)$, **3**, $Re_2(CO)_6(PBu^t_3)(\mu\text{-}PBu^t_2)(\mu\text{-}H)$, **4**, and $Re_2(CO)_5(PBu^t_3)(PBu^t_2H)(\mu\text{-}PBu^t_2O)(\mu\text{-}H)$, **5**. Compounds **4** and **5** are electronically unsaturated by the amount of two electrons; namely, one of the metal atoms has an 18-electron configuration and the other metal atom has a 16-electron configuration. Compound **4** adds CO and the nitriles MeCN and PhCN, reversibly, to form the electronically saturated 1:1 adducts $Re_2(CO)_7(PBu^t_3)(\mu\text{-}PBu^t_2)(\mu\text{-}H)$, **6**, $Re_2(CO)_6(NCMe)(PBu^t_3)(\mu\text{-}PBu^t_2)(\mu\text{-}H)$, **7**, and $Re_2(CO)_6(NCPh)(PBu^t_3)(\mu\text{-}PBu^t_2)(\mu\text{-}H)$, **8**, respectively. ^{13}CO labeling studies have shown that the CO ligand that is added to **4** to form **6** is added at the electronically saturated metal atom and one of the originally coordinated CO ligands is shifted to the unsaturated metal atom. Compound **5** also adds 1 equiv of CO to form the complex $Re_2(CO)_6(PBu^t_3)(PBu^t_2H)(\mu\text{-}PBu^t_2O)(\mu\text{-}H)$, **9**.$^{13}CO$ labeling studies have shown that the added CO ligand was added to the unsaturated metal atom in this case. All of the new compounds were characterized structurally by single-crystal X-ray diffraction analyses.

Introduction

Coordination asymmetry in binuclear metal systems is a feature that can produce unusual properties and reactivity to the metal atoms.[1] Coordination asymmetry is most pronounced when the metal atoms have different coordination numbers.[2] The metal atoms in binuclear mixed-valence complexes often have significantly different reactivities at the two metal atoms,[3] and most reactions occur preferentially at an electronically unsaturated metal atom, if one is present. For example, Nocera has shown that hydrogen activation occurs at the unsaturated metal atom in certain binuclear mixed-valent metal complexes.[4] We have recently shown how an unsaturated metal atom can activate a neighboring metal atom and also facilitate alkyne additions to it to promote alkyne insertion reactions.[5] Coordination asymmetry also appears to be very important to the reactivity of metalloenzymes and multimetallic proteins.[6]

We now wish to report some unusual coordinatively unsaturated dirhenium carbonyl complexes containing bulky *tert*-butylphosphine ligands. Surprisingly, for one of the complexes the ligand additions occur preferentially at the metal atom that is coordinatively and electronically saturated. A preliminary report on this work has been published.[7]

Experimental Section

General Data. Unless indicated otherwise, all reactions were performed under an atmosphere of nitrogen. Reagent grade solvents were dried by the standard procedures and were freshly distilled prior to use. Infrared spectra were recorded on a Thermo Nicolet Avatar 360 FT-IR spectrophotometer. ^1H NMR and $^{31}P\{^1H\}$ NMR spectra were recorded on a Varian Mercury 400 spectrometer operating at 400.1 and 161.9 MHz, respectively. $^{13}C\{^1H\}$ NMR spectra were recorded on a Varian Mercury 300 spectrometer operating at 75.5 MHz. Proton and phosphorus decoupled $^{13}C\{^1H\}\{^{31}P\}$ NMR and the variable-temperature $^{13}C\{^1H\}$ NMR experiments were recorded on a Varian Innova 500 spectrometer operating at 125.8 MHz. $^{31}P\{^1H\}$ NMR spectra were externally referenced against 85% *ortho*-H_3PO_4. Mass spectrometric (MS) measurements performed by a direct-exposure probe using electron impact ionization (EI) were made on a VG 70S instrument. Electrospray mass spectrometric measurements were obtained on a MicroMass Q-Tof spectrometer. ^{13}CO (99% ^{13}C, <5% ^{18}O) and benzonitrile, PhCN (99.9%), were purchased from Aldrich and were used as received. Tri-*tert*-butyl phosphine, PBu^t_3, was purchased from Strem and was used without further purification. The tri-*tert*-butyl phosphine was handled under nitrogen and stored at −80 °C. NMR analysis of the PBu^t_3 showed that it was predominantly PBu^t_3, but GC-mass spectral analysis showed the presence of significant amounts of the impurites: $O{=}PBu^t_3$, $O{=}P(H)Bu^t_2$, and $O{=}P(OH)Bu^t_2$. $Re_3(CO)_{12}(\mu\text{-}H)_3$ was prepared according to the published procedure.[8] Product separations were performed by thin-layer chromatography (TLC) in air on Analtech 0.25 and 0.5 mm silica gel 60 Å F_{254} glass plates.

* Corresponding author. E-mail: Adams@mail.chem.sc.edu.

(1) (a) Okawa, H.; Furutachi, H.; Fenton, D. E. *Coord. Chem. Rev.* **1998**, *174*, 51–75. (b) Satcher, J. H.; Droege, M. W.; Weakle, T. J. R.; Taylor, R. T. *Inorg. Chem.* **1995**, *34*, 3317–3328.

(2) (a) Gavrilova, A. L.; Bosnich, B. *Inorg. Chim. Acta* **2003**, *352*, 24–30. (b) Bosnich, B. *Inorg. Chem.* **1999**, *38*, 2554–2562. (c) McCollum, D. G.; Yap, G. A. P.; Rheingold, A. L.; Bosnich, B. *J. Am. Chem. Soc.* **1996**, *118*, 1365–1379.

(3) (a) Lambert, E.; Chabut, B.; Chardon-Noblat, S.; Deronzier, A.; Chottard, G.; Bousseksou, A.; Tuchagues, J.-P.; Lagier, J.; Bardet, M.; Latour, J.-M. *J. Am. Chem. Soc.* **1997**, *119*, 9424−9437. (b) Herber, U.; Pechmann, T.; Weberndorfer, B.; Ilg, K.; Werner, H. *Chem.−Eur. J.* **2002**, *8*, 309–319.

(4) (a) Gray, T. G.; Veige, A. S.; Nocera, D. G. *J. Am. Chem. Soc.* **2004**, *126*, 9760–9768. (b) Veige, A. S.; Gray, T. G.; Nocera, D. G. *Inorg. Chem.* **2005**, *44*, 17–26.

(5) (a) Adams, R. D.; Captain, B.; Trufan, E.; Zhu, L. *J. Am. Chem. Soc.* **2007**, *129*, 7545–7556. (b) Adams, R. D.; Captain, B.; Zhu, L. *J. Am. Chem. Soc.* **2006**, *128*, 13672–13673.

(6) (a) Belle, C.; Pierrey, J. L. *Eur. J. Inorg. Chem.* **2003**, 4137–4146. (b) Feig, A. L.; Lippard, S. J. *Chem. Rev.* **41994**, *94*, 759–805. (c) Stenkamp, R. E. *Chem. Rev.* **1994**, *94*, 715–726.

(7) Adams, R. D.; Captain, B. *Angew. Chem., Int. Ed.* **2007**, *46*, 5714–5716.

(8) Kaesz, H. D.; Knox, S. A. R.; Koepke, J. W. R.; Saillant, B. *Chem. Commun.* **1971**, 477.

10.1021/om700790c CCC: $37.00
Publication on Web 11/21/2007

Reaction of $Re_3(CO)_{12}(\mu\text{-}H)_3$ with PBu^t_3. $Re_3(CO)_{12}(\mu\text{-}H)_3$ (50.3 mg, 0.056 mmol) and PBu^t_3 (50 μL, 0.201 mmol) were dissolved in 20 mL of octane. The reaction solution was heated to reflux for 6 h. After cooling, the solvent was then removed *in vacuo*, and the products were separated by TLC by using a 5:1 hexane/methylene chloride solvent mixture to yield in order of elution 1.1 mg (2% yield) of colorless $Re_2(CO)_8(\mu\text{-}PBu^t_2)(\mu\text{-}H)$, **1**, 2.5 mg (5% yield) of colorless $Re_2(CO)_7(\mu\text{-}PBu^t_2)(PBu^t_2H)(\mu\text{-}H)$, **2**, 1.3 mg (4%) of colorless $HRe(CO)_4(PBu^t_3)$, **3**, 15.4 mg (31% yield) of orange $Re_2(CO)_6(PBu^t_3)(\mu\text{-}PBu^t_2)(\mu\text{-}H)$, **4**, and 5.3 mg (9% yield) of yellow $Re_2(CO)_5(PBu^t_3)(PBu^t_2H)(\mu\text{-}PBu^t_2O)(\mu\text{-}H)$, **5**. Spectral data for $Re_2(CO)_8(\mu\text{-}PBu^t_2)(\mu\text{-}H)$, **1**: IR ν_{CO} (cm^{-1} in hexane): 2098 (w), 2074 (m), 1997 (vs), 1987 (s), 1969 (s), 1966 (m). ^1H NMR (400 MHz, d_8-toluene, rt, TMS): δ 1.25 (d, $^3J(P,H) = 14$ Hz, 18H; CH_3), −15.15 (d,$^2J(P,H) = 6$ Hz, hydride 1H). $^{31}P\{^1H\}$ NMR (162 MHz, d_8-toluene, rt, 85% *ortho*-H_3PO_4): δ 118 (s, 1P, μ-PBu^t_2). EI/MS: *m/z* 742 (M^+), 714 ($M^+ - CO$), 686 ($M^+ - 2CO$). The isotope pattern is consistent with the presence of two rhenium atoms. Spectral data for $Re_2(CO)_7(\mu\text{-}PBu^t_2)(PBu^t_2H)(\mu\text{-}H)$, **2**: IR ν (cm^{-1} in hexane): 2081 (m), 2024 (w), 1985 (m), 1975 (vs), 1954 (s), 1924 (m), 1918 (m), 1915 (m). ^1H NMR (400 MHz, d_8-toluene, rt, TMS): δ 4.77 (d,$^1J(P,H) = 333$ Hz, 1H, P-H),1.50 (d, $^3J(P,H) = 14$ Hz, 18 H; CH_3), 1.24 (d, $^3J(P,H) = 14$ Hz, 18H; CH_3), −15.00 (dd, $^2J(P,H) = 10$ Hz, $^2J(P,H) = 7$ Hz, hydride 1H). $^{31}P\{^1H\}$ NMR (162 MHz, d_8-toluene, rt, 85% *ortho*-H_3PO_4): δ 126 (d, $^2J(P,P) = 73$ Hz, 1P, μ-P*t*Bu_2), 33 (d, $^2J(P,P) = 70$ Hz, 1P, P*t*Bu_2H). EI/MS: *m/z* 860 (M^+), 832 ($M^+ - CO$), 804 ($M^+ - CO$), 804 ($M^+ - 3CO - H$). The isotope pattern is consistent with the presence of two rhenium atoms. Spectral data for $HRe(CO)_4(PBu^t_3)$, **3**: IR ν_{CO} (cm^{-1} in hexane): 2071 (m), 1979 (m), 1961 (s), 1956 (sh). ^1H NMR (400 MHz, d_8-toluene, rt, TMS): δ 1.21 (d, $^1J(P,H) = 13$ Hz, 27H, CH_3) −4.92 (d, $^2J(P,H) = 18$ Hz, hydride 1H). $^{31}P\{^1H\}$ NMR (162 MHz, d_8-toluene, rt, 85% *ortho*-H_3PO_4): δ 79 (s, 1P). EI/MS: *m/z* 501 ($M^+ - H$), 473 ($M^+ - H - CO$), 445 ($M^+ - H - 2CO$), 417 ($M^+ - H - 3CO$). The isotope pattern is consistent with the presence of one rhenium atom. Spectral data for $Re_2(CO)_6(PBu^t_3)(\mu\text{-}PBu^t_2)(\mu\text{-}H)$, **4**: IR ν_{CO} (cm^{-1} in hexane): 2079 (s), 1993 (vs), 1969 (vs), 1954 (vs), 1923 (s), 1850 (s). ^1H NMR (400 MHz, d_8-toluene, rt, TMS): δ 1.37 (d, $^3J(P,H) = 14$ Hz, 18H; CH_3), 1.24 (d, $^3J(P,H) = 12$ Hz, 27H; CH_3), −4.46 (dd, $^2J(P,H) = 12$ Hz, $^2J(P,H) = 5$ Hz, hydride 1H). $^{31}P\{^1H\}$ NMR (162 MHz, d_8-toluene, rt, 85% *ortho*-H_3PO_4): δ 139.68 (d, $^2J(P,P) = 99$ Hz, 1P, μ-P*t*Bu_2), 84.31 (d, $^2J(P,P) = 99$ Hz, 1P, P*t*Bu_3). $^{13}C\{^1H\}$ NMR 125.8 MHz, d_8-toluene): at −110 °C, 190.5 ppm (doublet, $^2J(P2,C) = 26$ Hz); at −40 °C, δ 204.5 (2C, t, $^2J(P1,C) = 5$ Hz, $^2J(P2,C) = 5$ Hz), 190.5 (1C, d, $^2J(P2,C) = 26$ Hz), 188.5 ppm (1C, d, $^2J(P2,C) = 8$ Hz), 187.9 (2C, d, $^2J(P2,C) = 5$ Hz); at 25 °C, 204.1, 190.2, 187.9; at 140 °C, 191.2. EI/MS: *m/z* 888 (M^+), 860 ($M^+ - CO$), 831 ($M^+ - 2CO - H$), 803 ($M^+ - 3CO - H$). The isotope pattern is consistent with the presence of two rhenium atoms. Spectral data for $Re_2(CO)_5(PBu^t_3)(PBu^t_2H)(\mu\text{-}PBu^t_2O)(\mu\text{-}H)$, **5**: IR ν_{CO} (cm^{-1} in hexane): 2023 (m), 1926 (vs), 1912 (s), 1909 (s), 1834 (s). ^1H NMR (400 MHz, $CDCl_3$, rt, TMS): δ 5.24 (dd, $^1J(P,H) = 339$ Hz, $^3J(P3,H) = 2$ Hz, 1H, P-H), 1.53 (d, $^3J(P,H) = 12$ Hz, 27H; CH_3, PBu^t_3), 1.44 (d, $^3J(P,H) = 14$ Hz, 18H; CH_3, PBu^t_2H), 1.25 (d, $^3J(P,H) = 13$ Hz, 18H; CH_3, μ-PBu^t_2O), −10.37 (ddd, $^2J(P1,H) = 26$ Hz, $^2J(P2,H) = 8$ Hz, $^2J(P3,H) = 12$ Hz, hydride 1H). $^{13}C\{^1H\}$ NMR (125.8 MHz, d_8-toluene, rt, TMS): δ 207.2 (s, br, 2C), 198.8 (s, br, 1C), 197.9 (s, br, 2C); at −60 °C, δ 208.4 (d, $^2J(P1,C) = 4$ Hz), 207.4 (d, $^2J(P1,C) = 6$ Hz), 199.7 (t, $^2J(P2,C) = 8$ Hz, $^2J(P3,C) = 8$ Hz), 199.3 (s), 196.5 (t, $^2J(P2,C) = 8$ Hz, $^2J(P3,C) = 8$ Hz). $^{31}P\{^1H\}$ NMR (162 MHz, $CDCl_3$, rt, 85% *ortho*-H_3PO_4): δ 138.4 (d, $^2J(P,P) = 114$ Hz, 1P, μ-PBu^t_2O), 76.5 (s, 1P, PBu^t_3), 34.0 (d, $^2J(P,P) = 114$ Hz, 1P, PBu^t_2H). NOTE: The ^1H NMR spectrum in d_8-toluene solvent shows that the CH_3 resonances of the μ-PBu^t_2O and PBu^t_2H ligands are overlapping. EI/MS: *m/z* 1022 (M^+), 965 ($M^+ - 2CO - H$), 937 ($M^+ - 3CO - H$), 909 ($M^+ - 4CO - H$), 853 ($M^+ - 6CO - H$). The isotope pattern is consistent with the presence of two rhenium atoms.

Preparation of $Re_2(CO)_7(PBu^t_3)(\mu\text{-}PBu^t_2)(\mu\text{-}H)$, 6. Carbon monoxide gas (1 atm) was bubbled through a solution of **4** (15.4 mg, 0.017 mmol) in 20 mL of hexane. Within a few minutes the orange-colored solution turned to yellow and then almost colorless. The CO gas was purged through this solution for a total of 10 min, and an IR spectrum after this time indicated complete conversion of the starting material **4**. The solvent was removed *in vacuo*, and the product was separated by TLC by using a 5:1 hexane/methylene chloride solvent mixture to yield 15.4 mg (97%) of colorless **6**. Spectral data for **6**: IR ν_{CO} (cm^{-1} in hexane): 2079 (m), 2018 (w), 1983 (m), 1974 (vs), 1953 (s), 1914 (m), 1908 (m). ^1H NMR (400 MHz, d_8-toluene, rt, TMS): δ 1.53 (d, $^3J(P,H) = 14$ Hz, 18H; CH_3), 1.38 (d, $^3J(P,H) = 12$ Hz, 27H; CH_3), −14.01 (dd, $^2J(P,H) = 15$ Hz, $^2J(P,H) = 8$ Hz, hydride 1H). $^{31}P\{^1H\}$ NMR (162 MHz, d_8-toluene, rt, 85% *ortho*-H_3PO_4): δ 120.84 (d, $^2J(P,P) = 71$ Hz, 1P, μ-PBu^t_2), 63.05 (d, $^2J(P,P) = 71$ Hz, 1P, PBu^t_3). The isotope pattern is consistent with the presence of two rhenium atoms. The assignments of the respective ^{31}P resonances were appropriately made from the selective phosphorus decoupled $^1H\{^{31}P\}$ NMR experiments, which showed the doublet at 1.53 ppm collapse into a singlet when the resonance at 120.84 ppm in the ^{31}P spectrum was irradiated. Accordingly, the doublet at 1.38 ppm collapsed into a singlet when the resonance at 63.05 ppm in the ^{31}P spectrum was irradiated. EI/MS: *m/z* 916 (M^+), 888 ($M^+ - CO$), 860 ($M^+ - 2CO$), 831 ($M^+ - 3CO - H$), 803 ($M^+ - 4CO - H$). The isotope pattern is consistent with the presence of two rhenium atoms.

Conversion of 6 to 4. Compound **6** (15.0 mg, 0.016 mmol) in 10 mL of heptane was heated to reflux for 1½ h. IR at this time showed complete conversion of the starting material **6** to **4**. The solvent was removed *in vacuo*, and the product was separated by TLC by using a 5:1 hexane/methylene chloride solvent mixture to yield 14.0 mg (96%) of orange **4**.

Preparation of ^{13}CO-Enriched $Re_2(CO)_7(PBu^t_3)(\mu\text{-}PBu^t_2)(\mu\text{-}H)$, 6. A 15.0 mg amount of **4** was dissolved in 25 mL of heptane in a 100 mL sidearm flask. The flask was evacuated and then filled with ^{13}CO. This solution was stirred for 30 min at room temperature, during which time the color of the solution turned from orange to almost colorless, affording ^{13}CO-enriched $Re_2(CO)_7(PBu^t_3)(\mu\text{-}PBu^t_2)(\mu\text{-}H)$, **6**. The ^{13}CO gas was then removed and the heptane solution heated to reflux for 1½ h under a purge of nitrogen to afford ^{13}CO-enriched $Re_2(CO)_6(PBu^t_3)(\mu\text{-}PBu^t_2)(\mu\text{-}H)$, **4**. The flask was then cooled to room temperature, evacuated, filled again with ^{13}CO, and stirred for 30 min at room temperature. These series of steps were repeated three times to increase the enrichment. The heptane solvent was then removed *in vacuo*, and the ^{13}CO-enriched **6** was purified by TLC by using a 5:1 hexane/methylene chloride solvent mixture.

Selective Addition of ^{13}CO to 4. A sample of **4** (15.0 mg, 0.017 mmol) containing CO ligands at the natural abundance level was dissolved in approximately 0.5 mL of toluene-d_8 in a 5 mm NMR tube and sealed with a rubber septum. The NMR tube was evacuated and filled with ^{13}CO. The NMR tube was shaken, and within minutes the orange-colored solution turned almost colorless. The $^{13}C\{^1H\}$ NMR spectrum at this time showed only one significant resonance at 187.2 ppm.

Preparation of ^{13}CO-Enriched $Re_2(CO)_6(PBu^t_3)(\mu\text{-}PBu^t_2)(\mu\text{-}H)$, 4. A sample of **6** enriched with ^{13}CO to approximately 30%, as described above, was dissolved in 10 mL of heptane and heated to reflux for 1½ h. The solvent was removed *in vacuo*, and the product was purified by TLC by using a 5:1 hexane/methylene chloride solvent mixture. A mass spectrum of the product **4** showed that it was enriched with ^{13}CO in the amount of approximately 30%.

Preparation of $Re_2(CO)_6(NCMe)(PBu^t_3)(\mu\text{-}PBu^t_2)(\mu\text{-}H)$, 7. Compound **4** (9.9 mg, 0.011 mmol) was dissolved in approximately 0.6 mL of acetonitrile (NCMe) in a medium vial (1 dram size, 3.7 mL). The solution was then concentrated to about half the volume and placed in a freezer at −25 °C for ∼ 2 days to yield 8.5 mg (82% yield) of light yellow-colorless crystals of **7**. Spectral data for **7**: IR ν_{CO} (cm^{-1} in acetonitrile): 2018 (w), 2000 (s), 1909 (vs), 1889 (sh). ^1H NMR (400 MHz, CD_3CN, rt, TMS): δ 1.60 (d, $^3J(P,H) = 12$ Hz, 27H; CH_3), 1.50 (t, $^3J(P,H) = 13$ Hz, 18H; CH_3), −11.76 (dd, $^2J(P,H) = 16$ Hz, $^2J(P,H) = 9$ Hz, hydride 1H). $^{31}P\{^1H\}$ NMR (162 MHz, CD_3CN, rt, 85% *ortho*-H_3PO_4): δ 114.09 (d, $^2J(P,P) = 67$ Hz, 1P, μ-P*t*Bu$_2$), 65.26 (d, $^2J(P,P) = 67$ Hz, 1P, PBu^t_3); ^{13}C NMR (125.8 MHz, d_8-toluene, rt, TMS): δ 203.1 (br), 201.9 (br), 200.1 (s), 196.8 (d, $^2J(P2,C) = 39$ Hz), 196.2 (s), 193.5 (d, $^2J(P2,C) = 9$ Hz). When the ^1H NMR spectrum was recorded on a 300 MHz instrument, the triplet at 1.50 ppm (overlapping doublet of doublets) splits into a doublet of doublets. ES^+/MS: *m*/*z* 929 (M^+), 887 (M^+ − NCMe − H). The isotope pattern is consistent with the presence of two rhenium atoms. NOTE: Compound **7** was rapidly converted back to **4** when **7** was dissolved in any solvent other than acetonitrile.

Preparation of $Re_2(CO)_6(NCPh)(PBu^t_3)(\mu\text{-}PBu^t_2)(\mu\text{-}H)$, 8. Compound **4** (10.0 mg, 0.011 mmol) was dissolved in a few drops of CH_2Cl_2 in a small vial (¼ dram size, 0.9 mL). A few drops of benzonitrile was added, and the vial was then shaken. Immediately, the orange-colored solution turned yellow. The vial was placed in a refrigerator at 8 °C for ∼5 days to yield 4.9 mg (44% yield) of light yellow crystals of **8**. IR ν_{CO} (cm^{-1} in benzonitrile): 2018 (m), 1999 (s), 1908 (vs, br). ^1H NMR (400 MHz, in ca. 0.5 mL of d_8-toluene and 0.1 mL of PhCN, rt, TMS): δ 1.68 (t, br, 18H; CH_3), 1.48 (d, $^3J(P,H) = 12$ Hz, 27H; CH_3), –11.60 (dd, $^2J(P,H) = 16$ Hz, $^2J(P,H) = 9$ Hz, hydride 1H). $^{31}P\{^1H\}$ NMR (162 MHz, in ca. 0.5 mLof d_8-toluene and 0.1 mL of PhCN, rt, 85% *ortho*-H_3PO_4): δ 114.4 (d, $^2J(P,P) = 68$ Hz, 1P, μ-PBu^t_2), 65.4 (d, $^2J(P,P) = 68$ Hz, 1P, PBu^t_3). Anal. Calcd: C, 39.95; H, 5.18. Found: C, 39.96; H 4.97.

Preparation of $Re_2(CO)_6(PBu^t_3)(PBu^t_2H)(\mu\text{-}PBu^t_2O)(\mu\text{-}H)$, 9. Compound **5** (10.2 mg, 0.010 mmol) was dissolved in approximately 0.6 mL of hexane in a 10 mL Schlenk tube. CO gas was passed through the tube for 15 min, and the orange-colored solution turned yellow. The Schlenk tube was then sealed under an atmosphere of CO and placed in a freezer (−80 °C) overnight. A total of 6.0 mg (57% yield) of compound **9** crystallized and was collected. Spectral data for **9**: IR ν_{CO} (cm^{-1} in hexane): 2038 (m), 2019 (w), 1939 (vs), 1917 (s), 1912 (s), 1901 (m), 1885 (m), 1875 (m). ^1H NMR (400 MHz, d_8-toluene, rt, TMS): δ 4.82 (d, $^1J(P,H) = 331$ Hz, 1H, P-H), 1.44 (d, $^3J(P,H) = 12$ Hz, 27H; CH_3, PBu^t_3), 1.42 (d, $^3J(P,H) = 13$ Hz, 18H; CH_3, PBu^t_2O), 1.33 (d, $^3J(P,H) = 14$ Hz, 18H; CH_3,μ-PBu^t_2H), −17.95 (ddd, $^2J(P1,H) = 17$ Hz, $^2J(P2,H) = 8$ Hz, $^2J(P3,H) = 5$ Hz, hydride 1H). $^{31}P\{^1H\}$ NMR (162 MHz, $CDCl_3$, rt, 85% *ortho*-H_3PO_4): δ 115.9 (d, $^2J(P,P) = 110$ Hz, 1P, μ-PBu^t_2O), 71.3 (s, 1P, PBu^t_3), 32.9 (d, $^2J(P,P) = 111$ Hz, 1P, PBu^t_2H). Anal. Calcd: C, 38.85; H, 6.23. Found: C, 38.63; H, 5.96. When a solution of **9** was placed under an atmosphere of ^{13}CO at room temperature, all CO ligand sites were rapidly and equally enriched with ^{13}CO. ^{13}C NMR (125 MHz, d_8-toluene, rt, TMS): δ 199.0 (t, $^2J(P2,C) = 8$ Hz, $^2J(P3,C) = 8$ Hz), 196.8 (d, $^2J(P1,C) = 6$ Hz), 194.8 ppm (s).

Crystallographic Analyses. Colorless single crystals of **1**, **2**, and **3**, red single crystals of **4**, and orange single crystals of **5** suitable for X-ray diffraction analyses were obtained by slow evaporation of solvent from a hexane/methylene chloride solvent mixture at −25 °C. Colorless single crystals of **6** were obtained by slow evaporation of diethyl ether at −25 °C. Colorless single crystals of **7** were obtained by slow evaporation from a acetonitrile solution at −25 °C. Colorless single crystals of **8** were obtained by slow evaporation from a methylene choride/benzonitrile solution at 8 °C. Yellow single crystals of **9** were grown at −25 °C under an atmosphere of CO in hexane solvent. Each data crystal was glued onto the end of a thin glass fiber. X-ray intensity data were measured by using a Bruker SMART APEX CCD-based diffractometer using Mo Kα radiation ($\lambda = 0.71073$ Å). The raw data frames were integrated with the SAINT+ program by using a narrow-frame integration algorithm.[9] Corrections for Lorentz and polarization effects were also applied with SAINT+. An empirical absorption correction based on the multiple measurement of equivalent reflections was applied using the program SADABS. All structures were solved by a combination of direct methods and difference Fourier syntheses and refined by full-matrix least-squares on F^2, by using the SHELXTL software package.[10] All nonhydrogen atoms were refined with anisotropic displacement parameters. Hydrogen atoms were placed in geometrically idealized positions and included as standard riding atoms during the least-squares refinements. Crystal data, data collection parameters, and results of the analyses are listed in Tables 1, 2, and 3.

All compounds except for compounds **2** and **4** crystallized in the monoclinic crystal system. For compounds **1** and **3** the systematic absences in the intensity data were consistent with the unique space group $P2_1/n$. The hydrido ligands in both compounds were located and refined successfully with isotropic thermal parameters. For compound **5** the systematic absences in the intensity data were consistent with either of the space groups *Cc* or *C*2/*c*, the latter of which was confirmed by the successful solution and refinement of the structure. The hydrido ligand was located and refined on its positional parameters with a fixed isotropic thermal parameter. The hydrogen atom on the PBu^t_2H group was located and refined successfully with isotropic thermal parameters. The crystal packing of the molecules of **5** contains voids that are filled with disordered molecules from cocrystallization of solvent. Despite many attempts, no reasonable disorder model for these solvent molecules could be obtained. In the final stages of the refinements the largest peak in the final difference Fourier map was 2.320 $e^-/Å^3$, with satisfactory low *R* factors, $R_1 = 4.58\%$. For compounds **6**, **7**, and **9** the systematic absences in the intensity data were consistent with the unique space group $P2_1/c$. The hydrido ligands in compounds **6** and **7** were located and refined successfully with isotropic thermal parameters. For compound **9** all the atoms of the PBu^t_2H group were disordered over two orientations and were refined in the ratio 50/50. The carbon atoms were refined with isotropic thermal parameters. The hydrido ligand and the hydrogen atom on the PBu^t_2H ligand were both located and refined with a fixed isotropic thermal parameter. For compound **8** the systematic absences in the intensity data were consistent with either of the space groups $P2_1/m$ or $P2_1$. The structure could be solved only in the latter space group. The hydrido ligand was located and refined on its positional parameters with a fixed isotropic thermal parameter.

Compound **2** crystallized in the triclinic crystal system. The space group $P\bar{1}$ was assumed and confirmed by the successful refinement and solution of the structure. The hydrido ligand and the hydrogen atom on the PBu^t_2H group were located and refined successfully with isotropic thermal parameters.

Compound **4** crystallized in the orthorhombic crystal system. The systematic absences in the intensity data were consistent with either of the space groups *Pnma* or *Pna*2_1. The structure could only be solved in the latter space group. The hydrido ligand was located and refined successfully with an isotropic thermal parameter.

Molecular Orbital Calculations. A single-point molecular orbital calculation on **4** was performed on the molecular structure as derived from the single-crystal X-ray diffraction analysis. PH_3 was used in place of PBu^t_3 in these calculations. The P−H distance that was used was 1.41 Å. The molecular orbital calculations

(9) *SAINT+*; Bruker Analytical X-ray System, Inc.: Madison, WI, 2001.

(10) Sheldrick, G M. *SHELXTL* Version 6.1; Bruker Analytical X-ray Systems, Inc.: Madison, WI, 1997.

Table 1. Crystallographic Data for Compounds 1, 2, and 3

	1	2	3
empirical formula	$Re_2PO_8C_{16}H_{19}$	$Re_2P_2O_7C_{23}H_{38}$	$RePO_4C_{16}H_{28}$
fw	742.68	860.87	501.55
cryst syst	monoclinic	triclinic	monoclinic
lattice params			
a (Å)	8.9014(2)	9.1219(2)	8.0633(5)
b (Å)	16.2671(3)	12.8748(3)	29.2329(17)
c (Å)	14.7419(3)	12.9356(3)	8.4785(5)
α (deg)	90	91.103(1)	90
β (deg)	94.751(1)	99.360(1)	106.308(1)
γ (deg)	90	95.351(1)	90
V (Å^3)	2127.29(8)	1491.52(6)	1918.1(2)
space group	$P2_1/n$ (#14)	$P\bar{1}$ (#2)	$P2_1/n$ (#14)
Z value	4	2	4
ρ_{calc} (g/cm^3)	2.319	1.917	1.737
μ(Mo Kα) (mm^{-1})	11.482	8.251	6.432
temperature (K)	294(2)	294(2)	294(2)
$2\theta_{max}$ (deg)	56.64	56.60	56.58
no. obsd ($I > 2\sigma(I)$)	4557	6244	3776
no. params	254	327	212
goodness of fit (GOF)	1.034	1.085	1.091
max. shift in cycle	0.001	0.001	0.001
residuals:[a] R1; wR2	0.0208; 0.0484	0.0240; 0.0569	0.0332;0.0805
absor corr, max./min.	multi-scan 1.000/0.535	multiscan 1.000/0.511	multiscan 1.000/0.597
largest peak in final diff map (e$^-$/Å^3)	0.780	1.358	1.127

[a] $R = \sum_{hkl}(|F_{obs}| - |F_{calc}|)/\sum_{hkl}|F_{obs}|$; $R_w = [\sum_{hkl}w(|F_{obs}| - |F_{calc}|)^2/\sum_{hkl}wF_{obs}^2]^{1/2}$, $w = 1/\sigma^2(F_{obs})$; GOF $= [\sum_{hkl}w(|F_{obs}| - |F_{calc}|)^2/(n_{data} - n_{vari})]^{1/2}$.

Table 2. Crystallographic Data for Compounds 4, 5, and 6

	4	5	6
empirical formula	$Re_2P_2O_6C_{26}H_{46}$	$Re_2P_3O_6C_{33}H_{65}$	$Re_2P_2O_7C_{27}H_{46}$
fw	888.97	1023.16	916.98
cryst syst	orthorhombic	monoclinic	monoclinic
lattice params			
a (Å)	21.1976(10)	51.0915(17)	16.4619(4)
b (Å)	17.2257(8)	8.7205(3)	11.8441(3)
c (Å)	8.8901(4)	19.8896(7)	16.9897(4)
β (deg)	90	97.067(1)	93.057(1)
V (Å^3)	3246.2(3)	8794.4(5)	3307.88(14)
space group	$Pna2_1$(#33)	$C2/c$ (#15)	$P2_1/c$ (#14)
Z value	4	8	4
ρ_{calc} (g/cm^3)	1.819	1.546	1.841
μ(Mo Kα) (mm^{-1})	7.583	5.644	7.441
temperature (K)	294	294(2)	294
$2\theta_{max}$ (deg)	56.90	56.60	56.62
no. obsd ($I > 2\sigma(I)$)	7338	7897	7468
no. params	345	425	362
goodness of fit (GOF)	1.078	1.037	1.061
max. shift in cycle	0.002	0.005	0.001
residuals:[a] R1; wR2	0.0279; 0.0626	0.0458; 0.1274	0.0217; 0.0539
absorp corr, max./min.	multiscan 1.000/0.512	multiscan 1.000/0.569	multiscan 1.000/0.582
largest peak in final diff map (e$^-$/Å^3)	2.390	2.320	1.588

[a] $R = \sum_{hkl}(|F_{obs}| - |F_{calc}|)/\sum_{hkl}|F_{obs}|$; $R_w = [\sum_{hkl}w(|F_{obs}| - |F_{calc}|)^2/\sum_{hkl}wF_{obs}^2]^{1/2}$, $w = 1/\sigma^2(F_{obs})$; GOF $= [\sum_{hkl}w(|F_{obs}| - |F_{calc}|)^2/(n_{data} - n_{vari})]^{1/2}$.

reported herein were performed by using the Fenske–Hall method. Contracted double-ζ basis sets were used for the Re 5d, P 3p, and C and O 2p atomic orbitals. The Fenske–Hall molecular orbital method is an approximate self-consistent-field (SCF) nonempirical method that is capable of calculating molecular orbitals for very large transition metal systems and has built-in fragment analysis routines that allow one to assemble transition metal cluster structures from the ligand-containing fragments.

Results and Discussion

Five new complexes were obtained from the reaction of $Re_3(CO)_{12}(\mu\text{-H})_3$ with PBu^t_3 in solution in octane solvent at reflux (127 °C) for 6 h. These have been identified as $Re_2(CO)_8(\mu\text{-}PBu^t_2)(\mu\text{-H})$, **1**, in 2% yield, $Re_2(CO)_7(\mu\text{-}PBu^t_2)(PBu^t_2H)(\mu\text{-H})$, **2**, in 5% yield, $HRe(CO)_4(PBu^t_3)$, **3**, in 4% yield, $Re_2(CO)_6(PBu^t_3)(\mu\text{-}PBu^t_2)(\mu\text{-H})$, **4**, in 31% yield, and $Re_2(CO)_5(PBu^t_3)(PBu^t_2H)(\mu\text{-}PBu^t_2O)(\mu\text{-H})$, **5**, in 9% yield. All five compounds were characterized by a combination of IR, ^{1}H and ^{31}P{1H} NMR, and single crystal X-ray diffraction analyses.

An ORTEP showing the molecular structure of compound **1** is shown in Figure 1. This molecule is a dinuclear complex that contains two rhenium atoms with a PBu^t_2 ligand and a hydrido ligand that bridge the Re−Re bond on opposite sides. The molecule is structurally similar to the compound $Re_2(CO)_8(\mu\text{-}PPh_2)(\mu\text{-H})$, which has a bridging diphenylphosphido ligand instead of a di-*tert*-butyl phosphido ligand.[12] The Re−Re distance in **1**, Re1−Re2 = 3.1291(2) Å, is similar in length to

(11) (a) Hall, M. B.; Fenskey, R. F. *Inorg. Chem.* **1972**, *11*, 768–775. (b) Webster, C. E.; Hall, M. B. In *Theory and Applications of Computational Chemistry: The First Forty Years*; Dykstra, C., Ed.; Elsevier: Amsterdam, 2005; Chapter 40, pp 1143–1165. (c) Manson, J.; Webster, C. E.; Perez, L. M.; Hall, M. B. http://www.chem.tamu.edu/jimp2/index.html.

(12) Florke, U.; Haupt, H.-J. *Z. Kristallogr.* **1994**, *209*, 702.

Table 3. Crystallographic Data for Compounds 7, 8, and 9

	7	8	9
empirical formula	$Re_2P_2O_6N_1C_{28}H_{49}$	$Re_2P_2O_6N_1C_{33}H_{51}$	$Re_2P_3O_7C_{34}H_{65}$
fw	930.02	992.09	1051.17
cryst syst	monoclinic	monoclinic	monoclinic
lattice params			
a (Å)	11.0279(4)	11.8592(3)	19.3906(7)
b (Å)	29.6026(10)	11.2504(3)	12.4072(5)
c (Å)	10.7886(3)	14.1065(4)	17.2721(8)
β (deg)	105.577(1)	94.708(1)	91.314(1)
V (Å^3)	3392.63(19)	1875.75(9)	4154.3(3)
space group	$P2_1/c$ (#14)	$P2_1$ (#4)	$P2_1/c$ (#14)
Z value	4	2	4
ρ_{calc} (g/cm^3)	1.821	1.757	1.681
μ(Mo Kα) (mm^{-1})	7.261	6.573	5.978
temperature (K)	294	294(2)	294(2)
$2\theta_{max}$ (deg)	56.60	56.56	52.04
no. obsd ($I > 2\sigma(I)$)	7412	8830	7154
no. params	356	400	422
goodness of fit (GOF)	1.101	1.055	1.298
max. shift in cycle	0.002	0.002	0.001
residuals:[a] R1; wR2	0.0227; 0.0532	0.0174; 0.0487	0.0490; 0.1141
absorp corr, max./min.	multiscan 1.000/0.832	multiscan 1.000/0.631	multiscan 1.000/0.433
largest peak in final diff map (e$^-$/Å^3)	1.201	0.865	1.631

[a] $R = \sum_{hkl}(|F_{obs}| - |F_{calc}|)/\sum_{hkl}|F_{obs}|$; $R_w = [\sum_{hkl}w(|F_{obs}| - |F_{calc}|)^2/\sum_{hkl}wF_{obs}^2]^{1/2}$, $w = 1/\sigma^2(F_{obs})$; GOF $= [\sum_{hkl}w(|F_{obs}| - |F_{calc}|)^2/(n_{data} - n_{vari})]^{1/2}$.

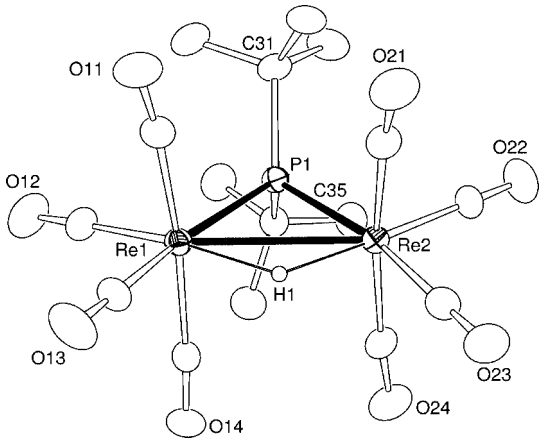

Figure 1. ORTEP showing the molecular structure of **1** at 30% thermal ellipsoid probability. Selected interatomic bond distances (Å) and angles (deg) are as follows: Re1−Re2 = 3.1291(2), Re1−H1 = 1.88(4), Re2−H1 = 1.84(4), Re1−P1 = 2.4906(9), Re2−P1 = 2.4975(9), Re1−P1−Re2 = 77.70(2).

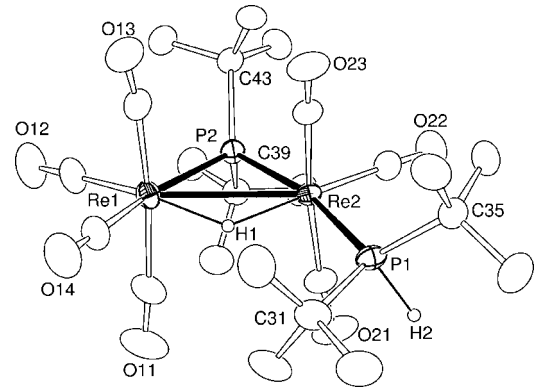

Figure 2. ORTEP showing the molecular structure of **2** at 30% thermal ellipsoid probability. Selected interatomic bond distances (Å) and angles (deg) are as follows: Re1−Re2 = 3.1524(2), Re1−H1 = 1.81(6), Re2−H1 = 1.80(6), Re1−P2 = 2.4924(10), Re2−P2 = 2.4530(10), Re2−P1 = 2.4492(10), P1−H2 = 1.50(5), Re1−P2−Re2 = 79.20(3).

that found in $Re_2(CO)_8(\mu\text{-}PPh_2)(\mu\text{-H})$, Re−Re = 3.165 Å. The hydrido ligand was located and refined structurally, and it exhibits the usual high-field resonance, $\delta = -15.15$ ppm, in its ^{1}H NMR spectrum. The complex is electronically saturated, as both rhenium atoms have an 18-electron configuration. The bridging di-*tert*-butyl phosphido ligand was apparently formed by the cleavage of one *tert*-butyl group of a molecule of PBu^t_3. Several of the other products also contain a bridging di-*tert*-butyl phosphido ligand; see below.

Compound **2** was characterized crystallographically, and an ORTEP diagram of its molecular structure is shown in Figure 2. Compound **2** is also a dirhenium complex containing a bridging PBu^t_2 ligand and a bridging hydrido ligand as found in **1**. The hydrido ligand was located and refined crystallographically. It exhibits the usual high-field ^{1}H NMR signal, $\delta = -15.00$, with coupling to both phosphorus atoms (^2J(P,H) = 10 Hz, ^2J(P,H) = 7 Hz, hydride 1H). In addition, there is a terminal PBu^t_2H ligand on one of the rhenium atoms, Re2, in place of one of the CO ligands in **1**. The presence of a hydrogen atom on the phosphorus atom of the terminal di-*tert*-butyl phosphine ligand was confirmed by the ^{1}H NMR spectrum, which showed a doublet at 4.77 ppm with appropriate one-bond coupling to ^{31}P, ^1J(P,H) = 333 Hz. This chemical shift and coupling constant are in good agreement with the ^{1}H NMR spectrum of the PBu^t_2H ligand found in the compound $FeIr(\mu\text{-}CO)(CO)_4(\mu\text{-}PBu^t_2)(PBu^t_2H)$.[13] Compound **2** is also saturated, having a total of 34 valence electrons with a Re−Re single bond between the two metal atoms. The PBu^t_2H ligand may have been formed by the elimination of isobutene from PBu^t_3, but this has not been confirmed. Such a process might have led to the formation of the bridging PBu^t_2 ligand and a bridging hydrido ligand in compounds **1** and **2** and in **4** too; see below.

An ORTEP diagram showing the molecular structure of compound **3** is presented in Figure 3. Compound **3** is a six-coordinate mononuclear rhenium complex having a pseudo-octahedral arrangement of ligands. The complex has four terminal carbonyl ligands, one terminal PBu^t_3 ligand, and one terminal hydrido ligand that is located *cis* to the PBu^t_3 ligand. It is structurally similar to the diphenyl(methoxy)phosphine

(13) Böttcher, H.-C.; Graf, M.; Merzweiler, K *J. Organomet. Chem.* **1996**, *525*, 191–197.

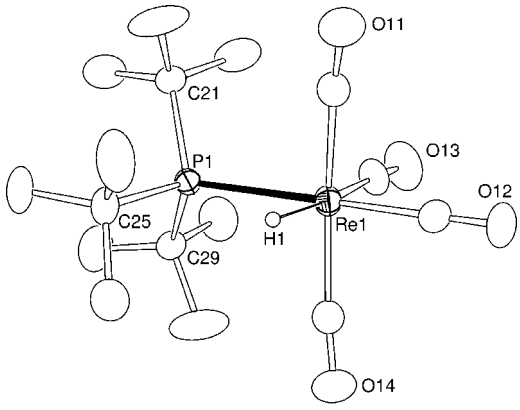

Figure 3. ORTEP showing the molecular structure of **3** at 30% thermal ellipsoid probability. Selected interatomic bond distances (Å) and angles (deg) are as follows: Re1−H1=1.62(4), Re1−P1 = 2.5795(12), P1−Re1−H1 = 77.4(16), C12−Re1−P1 = 173.82(18).

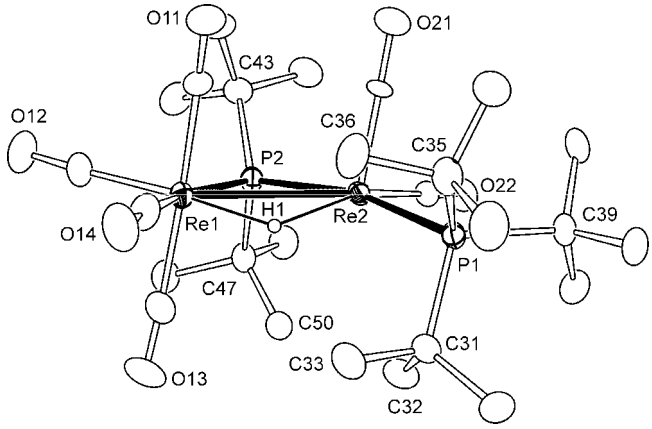

Figure 4. ORTEP showing the molecular structure of **4** at 30% thermal ellipsoid probability. Selected interatomic bond distances (Å) and angles (deg) are as follows: Re1−Re2 = 3.1083(3), Re1−P2 = 2.4874(13), Re2−P2 = 2.4175(13), Re2−P1 = 2.4831(13), Re1−H1 = 1.76(5), Re2−H1 = 2.02(5); C31−P1−Re2 = 103.65(19), C35−P1−Re2 = 116.0(2), C39−P1−Re2 = 113.3(2).

complex HRe(CO)$_4${PPh$_2$(OMe)}.[14] The hydrido ligand in **3** was located and refined structurally. The Re1−H1 bond distance, 1.62(4) Å, is similar to the Re−H bond distance, 1.60(8) Å, found in HRe(CO)$_4${PPh$_2$(OMe)}. The hydrido ligand exhibits the characteristic high-field resonance, δ = –4.92, in the ^{1}H NMR spectrum with appropriate coupling to the phosphine ligand, ^2J(P−H) = 18 Hz.

An ORTEP drawing of the molecular structure of **4**, the major product of this reaction, is shown in Figure 4. The parent ion in the mass spectrum, *m/z* 888, confirms the molecular formula. This dirhenium complex contains a bridging PBu$^t_2$ ligand and a bridging hydrido ligand across a Re−Re bond, but unlike **1** and **2**, compound **4** has only seven additional ligands. Atom Re(1) has four CO ligands and Re(2) has two CO ligands and one PBu$^t_3$ ligand. Compound **4** is thus electron deficient by the amount of two electrons. Atom Re1 has an 18-electron configuration, and atom Re2 formally has a 16-electron configuration, and there is clear evidence for a vacant coordination site trans to the CO ligand C21−O21 on Re(2). This ligand-deficient

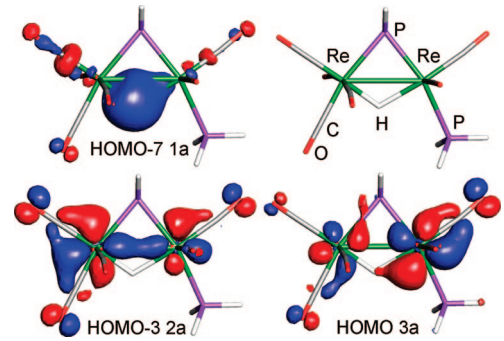

Figure 5. Contour diagrams for some selected Fenske–Hall molecular orbitals for **4**. HOMO−7 1a (−12.25 eV), HOMO−3 2a (−9.05 eV), HOMO 3a (−7.42 eV). A line structure showing the locations of the atoms in the diagrams is shown at the top right.

structure is stabilized by the bulky PBu$^t_3$ ligand P1. One of the *tert*-butyl groups, C31, partially occupies the vacant coordination site, as evidenced by the Re1−P1−C31 bond angle, C31−P1−Re2 = 103.65(19)°, which is 10° smaller than the C−P−Re angles to the other *tert*-butyl groups on P1, C35−P1−Re2 = 116.0(2)°, C39−P1−Re2 = 113.3(2)°. This could be evidence for a very weak agostic C−H interaction from methyl group C32, which makes the closest approach to Re2, Re2···C32 = 3.216 Å, although the hydrogen atoms on the methyl groups were not located in the structural analysis. The M−P−C angles involving M−PBu$^t_3$ groups with strong agostic interactions to the methyl groups are more acute, 96–99°, than that found in **4**.[15]

The hydrido ligand in **4** was located and refined crystallographically. It exhibits the characteristic high-field resonance in the ^{1}H NMR spectrum, δ = –4.46, with appropriate couplings to the two phosphine ligands, ^2J(P,H) = 12 Hz, ^2J(P,H) = 5 Hz, but its shift is much less than those of the bridging hydrido ligands in **1** and **2**. Although there are not many examples, there is clear evidence that electronic unsaturation can produce significant deshielding effects on bridging hydrido ligands. For example, the hydride resonances of the unsaturated complexes Re$_4$(CO)$_{12}$(μ_3-H)$_4$ and Os$_3$(CO)$_{10}$(μ-H)$_2$ are much less shielded than those of related saturated cluster complexes.[16] The Re−Re bond distance in **4**, Re1−Re2 = 3.1083(3) Å, is slightly shorter than the Re−Re bond distances in **1** and **2**. This may be due to a decrease in steric interactions about Re(2) because there are fewer ligands attached to it; however the bond is still significantly longer than the Re−Re bond in Re$_2$(CO)$_{10}$, 3.042(1) Å, which contains no bulky ligands.[17]

To develop a better understanding of the electronic structure of **4**, Fenske−Hall molecular orbital calculations were performed on the structure as found in the solid state. To simplify these calculations, each *tert*-butyl group was replaced by one hydrogen atom at the typical P−H bond distance of 1.41 Å. Contour diagrams of the most important occupied molecular orbitals found in **4** are shown in Figure 5. The HOMO 3a consists predominantly of π-bonding between the metal atoms and two of the CO ligands, but there is also a significant interaction between the hydrido ligand and one of the Re atoms, Re2. The Re−Re bond is represented by the HOMO−3 2a, and the bonding of the bridging hydrido ligand is represented best by

(14) Albertin, G.; Antoniutti, S.; Garcia-Fontán, S.; Carballo, R.; Padoan, F. *J. Chem. Soc., Dalton Trans.* **1998**, 2071–2081.

(15) Cooper, A. C.; Streib, W. E.; Eistenstein, O.; Caulton, K. G. *J. Am. Chem. Soc.* **1997**, *119*, 9069–9070.

(16) Humphries, A. P.; Kaesz, H. D. *Prog. Inorg. Chem.* **1979**, *25*, 145–222.

(17) Churchill, M. R.; Amoh, K. N.; Wasserman, H. J. *Inorg. Chem.* **1981**, *20*, 1609.

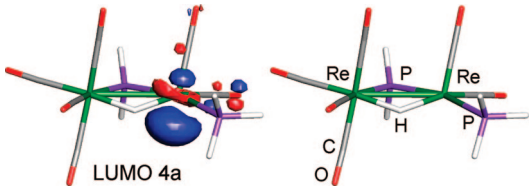

Figure 6. Contour diagram of the lowest unoccupied orbital LUMO 4a (−2.95 eV) in **4** is shown on the left. A line structure showing the orientation of the molecule and the locations of the atoms in the MO diagram is shown on the right.

the HOMO−7 1a. The most interesting orbital is the lowest unoccupied molecular orbital LUMO 4a. The major component of this orbital lies trans to the CO(21) ligand; see Figure 6. It clearly defines the so-called "vacant" site.

The $^{13}C\{^1H\}$ NMR spectrum of compound **4** shows only three broad resonances in the CO region, 204.1, 190.2, and 187.9 ppm at 25 °C. Suspecting dynamical activity, variable-temperature measurements were made and this was confirmed. A series of spectra of **4** recorded at several different temperatures are shown in Figure 7. At −40 °C four resonances were observed: a triplet at 204.5 ppm (2C) with small and equal coupling to the two phosphorus atoms, ^2J(P1,C) = 5 Hz, ^2J(P2,C) = 5 Hz; a doublet at 190.5 ppm (1C) with larger coupling to the bridging phosphido ligand P2, ^2J(P2,C) = 26 Hz; and a doublet at 188.5 ppm (1C) with small coupling to one of the phosphorus atoms, ^2J(P2,C) = 8 Hz, and 187.9 ppm (2C), d, ^2J(P2,C) = 5 Hz. The small P−C couplings cannot be seen in Figure 7. The resonance at 204.5 ppm is assigned to the two CO ligands on Re2, CO(21) and CO(22), which are still dynamically averaged at this temperature. The resonance at δ 190.5 is assigned to CO(14) on Re1. The resonance at 188.5 ppm is assigned to CO(12) on Re1. The resonance at 187.9 ppm is assigned to CO(11) and CO(13) on Re1. These ligands are still dynamically averaged at this temperature. As the temperature is lowered still further, the resonances at 204.5 and 187.9 ppm broaden and collapse into the baseline due to a slowing of the lower temperature exchange process. At −110 °C, two very broad resonances are beginning to resolve at 201 and 208 ppm for (CO)21 and (CO)22 and there is a very broad resonance in the baseline at 186 ppm for (CO)11 and (CO)13. The exchange process is very rapid, and one would have to go much lower in temperature to reach the slow exchange limit. The coalescence temperature for this process is estimated to be at −100 °C, and the rate of exchange at the coalescence temperature (k_c) was estimated by using the expression $k_c = \pi\Delta\nu_0/(2)^{1/2}$, where $\Delta\nu_0$ is the chemical shift difference between the maxima of the two broad resonances observed at −110 °C. Substitution of k_c in the Eyring equation provides the free energy of activation for the process at the coalescence temperature $\Delta G^{\ddagger}$ (at 173 K) = 7.3 kcal/mol. As the temperature is raised above −40 °C, all of the resonances begin to broaden at approximately the same rate. They have coalesced at about 108 °C. This broad resonance continues to sharpen up to 140 °C, the highest temperature that we could record. The changes are reversible. The broadening and averaging of the resonances in the range −40 to 140 °C is due to a second dynamical process leading to exchange of the CO ligands between the two metal atoms and complete averaging of all of the CO ligands.

The dynamical averaging observed in the variable-temperature ^{13}C NMR can be explained by the two mechanisms. The low-temperature process in the range −110 to −40 °C can be explained by the exchange mechanism A shown in Scheme 1. Through this process the vacant site oscillates back and forth

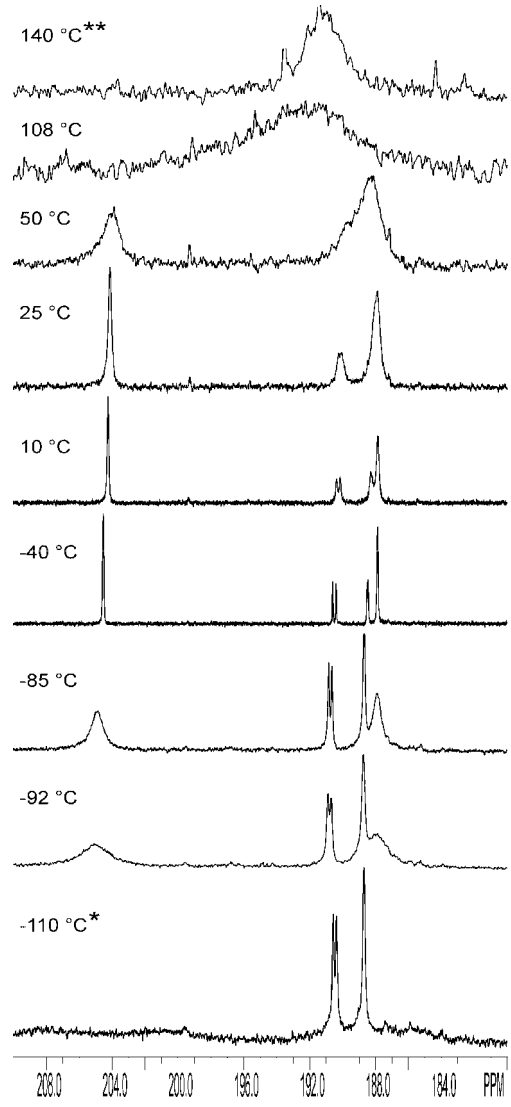

Figure 7. Variable-temperature $^{13}C\{^1H\}$ NMR spectra for compound **4** in d_8-toluene solvent. *The spectrum at −110 °C was recorded in diethyl ether solvent with a drop of CD_2Cl_2. **The spectrum at 140 °C was recorded in xylene solvent with a drop of d_8-toluene.

between the two sides of the Re_2P plane involving the bridging phosphido ligand. In this process the CO ligands 21 and 22 on Re2 exchange sites. As a consequence of this motion, the CO ligands 11 and 13 on Re1 also exchange their sites. The structure **4** is converted to its mirror image labeled as **4*** in Scheme 1. In the high-temperature CO exchange process, all of the CO ligands are exchanged. This requires the CO ligands to be exchanged between the two metal atoms. For this process we have adopted a 2 by 2 mechanism similar to that which was established for the bridging and terminal CO ligands in $[CpFe(CO)(\mu\text{-}CO)]_2$ many years ago.[18] This mechanism B is also shown in Scheme 1. In this process two CO ligands, 21 and 13, on opposite sides of the Re_2P plane shift into bridging positions to form the unobserved intermediate **4A**. These two CO ligands then shift to terminal positions on the other metal atoms, i.e., Re1 for 21 and Re2 for 13, to form the mirror image **4*** of the starting structure **4**. This completes the first iteration of the metal−metal exchange of the CO ligands. This structure can be converted to its mirror image **4** via the low-temperature

(18) Adams, R. D.; Cotton, F. A. *J. Am. Chem. Soc.* **1973**, *95*, 6589.

Scheme 1

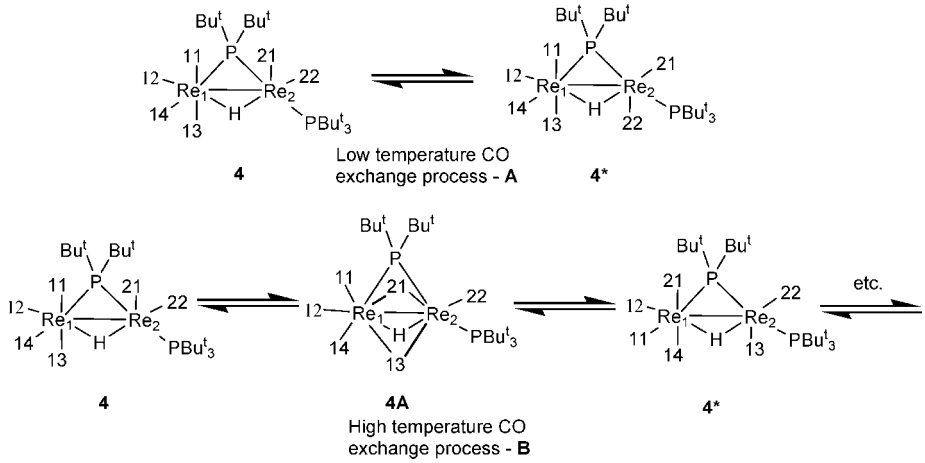

mechanism A, and then another pair of CO ligands, 22 and 14, could be exchanged between the metal atoms by the mechanism B. A similar process, not drawn, will lead to the exchange of CO 12 between the two metal atoms. Note: there is no experimental evidence of a distinction between the CO ligands 12 and 14 on Re_1; that is, both participate in this process. These cycles can repeat themselves until all CO ligands are exchanged.

The final product obtained from the reaction of $Re_3(CO)_{12}(\mu\text{-}H)_3$ with PBu^t_3 is the new compound $Re_2(CO)_5(PBu^t_3)(PBu^t_2H)(\mu\text{-}PBu^t_2O)(\mu\text{-}H)$, **5**. The molecular weight of **5** was confirmed by its mass spectrum, $m/z = 1022$. Compound **5** was also characterized by a single-crystal X-ray diffraction analysis, and an ORTEP diagram of the molecular structure of **5** is shown in Figure 8. This dirhenium complex contains a bridging di-*tert*-butylphosphidoxo ligand, $O{=}PBu^t_2$, and a bridging hydrido ligand across the Re−Re single bond, Re1−Re2 = 3.2048(4) Å. The longer length of the Re−Re bond can be explained by the presence of the less restrictive two-atom P−O bridge of the di-*tert*-butylphosphidoxo ligand. The Re−O distance, Re1−O1, is 2.067(5) Å. The Re−P distance is Re1−P1 = 2.457(2) Å. There are no reported structural characterizations of rhenium complexes containing bridging dialkyl- or diarylphosphidoxo ligands, but there are some polynuclear ruthenium complexes containing related phosphidoxo ligands.[19–21] The source of the oxygen atom bonded to the PBu^t_2 group in the bridging phosphidoxo ligand has not been definitively established. Mass spectral and ^{31}P NMR analyses of our PBu^t_3 reagent showed that it contained significant amounts of the phosphine oxide impurities $OPBu^t_3$ and $OP(H)Bu^t_2$.[22] It seems likely that the $O{=}PBu^t_2$ ligand in **5** was derived from one of these impurities. Diphenylphosphidoxo ligands have been obtained from phosphine oxide precursors previously.[19] The $O{=}PBu^t_2$ ligand serves as a three-electron donor. The P−O distance in **5**, P3−O1 = 1.587(5) Å, is significantly longer than that found in the free molecule $OP(H)Bu^t_3$,[22] where P−O = 1.4819(19) Å, but is similar to the P−O distances, 1.50–1.60 Å, observed for bridging phosphidoxo ligands in other ruthenium complexes.[19] The bridging hydrido ligand lies out of the Re1, Re2, P3 plane by 0.76(7) Å in the direction of CO(21), and this CO ligand is pushed away from it and from the Re−Re bond as shown by the large bond angle C21−Re2−Re1 = 111.3(2)°. By contrast CO(23) on the other side of the molecule moves toward the Re−Re bond, as shown by the acute angle C23−Re2−Re1 = 71.7(2)°. Although this angle is unusually acute, one should not infer that there is any significant bonding between the atoms C23 and Re1; in fact, the Re1···C23 distance of 3.198(1) Å is much too long to permit any significant direct bonding interaction between these two atoms. The resonance of the hydrido ligand occurs at δ −10.37, and it is coupled to all three phosphorus atoms, $^2J(P1,H) = 26$ Hz, $^2J(P2,H) = 8$ Hz, $^2J(P3,H) = 12$ Hz.

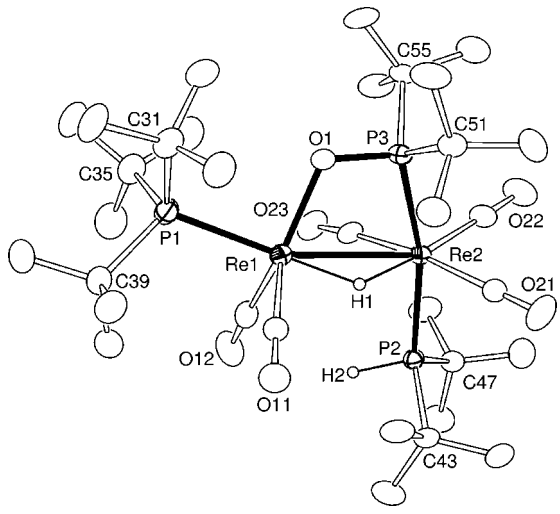

Figure 8. ORTEP showing the molecular structure of **5** at 30% thermal ellipsoid probability. Selected interatomic bond distances (Å) and angles (deg) are as follows: Re1−Re2 = 3.2048(4), Re1−O1 = 2.067(5), Re1−P1 = 2.457(2), Re1−H1 = 1.67(8), Re2−P3 = 2.4329(18), Re2−P2 = 2.4688(18), Re2−H1 = 1.93(7), P2−H2 = 1.39(6), Re1···C23 = 3.198, Re1···O23 = 3.745(1); P3−Re2−P2 = 165.56(6), O1−P3−Re2 = 105.19(19), P3−O1−Re1 = 115.4(3).

As with **4**, compound **5** contains only seven terminally coordinated ligands. Atom Re1 has two CO ligands and one PBu^t_3 ligand, and Re2 has three CO ligands and a PBu^t_2H ligand. Thus, like compound **4**, compound **5** is electron deficient by the amount of two electrons. This deficiency resides formally at atom Re1, which has a 16-electron configuration, but unlike **4** there is no well-defined vacant site on Re1. The ^{13}C NMR spectra of **5** were obtained by using a sample that was partially

(19) Fogg, D. E.; Taylor, N. J.; Meyer, A.; Carty, A. J. *Organometallics* **1987**, *6*, 2252.
(20) Bruce, M. I.; Humphrey, P. A.; Skelton, B. W.; White, A. H. *J. Organomet. Chem.* **1997**, *539*, 141–146.
(21) Bennett, D. W.; Siddiquee, T. A.; Haworth, D. T.; Kabir, S. E.; Hyder, M. I.; Ahmed, S. J. *J. Chem. Cryst.* **2004**, *34*, 361.
(22) Dornhaus, F.; Lerner, H.-W.; Bolte, M. *Acta Crystallogr.* **2005**, *E61*, o657–o658.

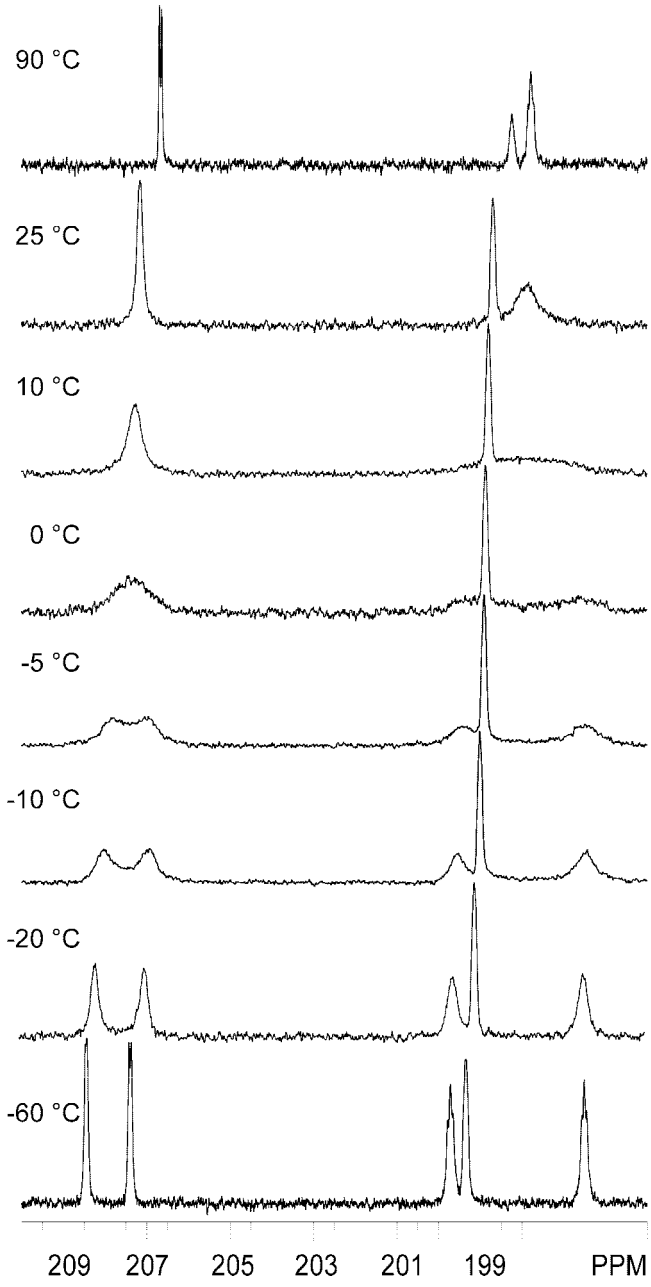

Figure 9. $^{13}C\{^1H\}$ NMR spectra at 125.8 MHz for compound **5** at various temperatures in d_8-toluene solvent.

enriched (~30%) with ^{13}CO. The ^{13}C NMR spectrum of **5** at room temperature exhibits three broad resonances at 207.2 (s, 2C), 198.8 (s, 1C), and 197.9 ppm (s, 2C). The broad resonances suggested dynamical activity, and so variable-temperature spectra were recorded. The $^{13}C\{^1H\}$ NMR spectra of compound **5** at various temperatures in the carbonyl region are shown in Figure 9. The limiting low-temperature spectrum was obtained at −60 °C. This spectrum exhibits five well-resolved resonances at δ = 208.4, 207.4, 199.7, 199.3, and 196.5, which correspond to the five CO ligands. The two resonances at 208.4 and 207.4 ppm are doublets with ^2J(P1,C) of 4 and 6 Hz, respectively. These resonances are assigned to the two CO ligands on Re1. The two resonances at 199.7 and 196.5 ppm are triplets and are assigned to the two CO ligands CO(21) and CO(23) on Re2. Both resonances show two-bond coupling to both P2 and P3 (^2J(P2,C) 8 Hz, ^2J(P3,C) 8 Hz). The resonance at 199.3 ppm does not exhibit any coupling to P2 or P3. Because of its similar chemical shift to CO(21) an CO(23), it is assigned to CO(22) on Re2. As the temperature is raised, the resonances at 208.4 and 207.4 ppm start to broaden and coalesce at 0 °C. Similarly, the resonances at 199.7 and 196.5 ppm start to broaden and coalesce at about +10 °C. The broadening of all four resonances is approximately the same, indicating that the rate of the exchange for the two averaging pairs of resonances is the same. The activation energy for the averaging process, $\Delta G^{\ddagger}$ (at 273 K) = 12.8 kcal/mol, was obtained from the coalescence temperature. As the temperature is raised to 90 °C, the resonances sharpen. The observation of P−C coupling in the fast exchange limit at 90 °C confirms that the exchange process is a nondissociative one. The resonance at 199.3 ppm assigned to (CO)22 showed no broadening throughout the entire temperature, and there was no evidence of exchange between the resonances of the CO ligands on Re1 with those on Re2.

Scheme 2

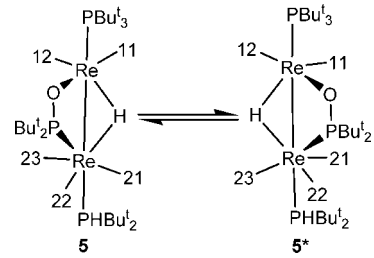

The simplest exchange process that would account for the pairwise exchange of the CO ligands on Re1 and Re2 is shown in Scheme 2. This involves a shift of the hydrido ligand to the other side of the Re−Re bond. CO(21) and CO(23) on Re2 will rock back and forth, but no bonds are broken. The first structure, **5**, is converted into its mirror image, **5***. The environments of ligands CO(11) and CO(12) on Re1 are exchanged as a consequence of the changes on Re2.

To investigate the properties of the ligand-deficient complex **4**, it was first treated with CO. The reaction of **4** with CO gas at 25 °C/1 atm was complete in a matter of minutes, and the product **6** was subsequently isolated in 97% yield. Compound **6** was characterized crystallographically, and an ORTEP diagram of its molecular structure is shown in Figure 10. Compound **6** is a CO adduct of **4**. The basic structure is the same as that of **4** except that there is an additional CO ligand on the metal atom Re2 that contains the PBu$^t_3$ ligand. Indeed, a terminal CO ligand,

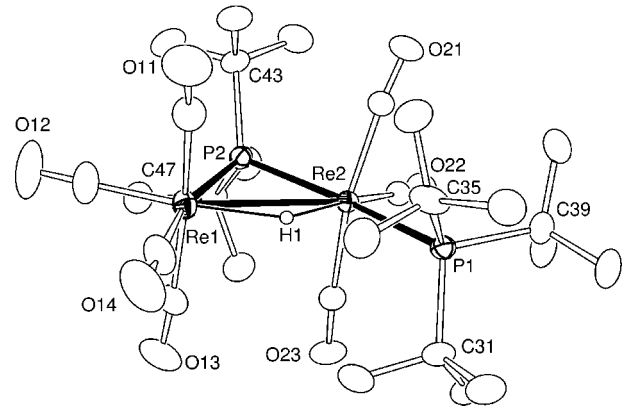

Figure 10. ORTEP of the molecular structure of **6** showing 30% thermal ellipsoid probability. Selected interatomic bond distances (Å) and angles (deg) are as follows: Re1−Re2 = 3.17813(18), Re1−P2 = 2.4871(9), Re2−P2 = 2.4461(8), Re2−P1 = 2.5931(8), Re1−H1 = 1.93(4), Re2−H1 = 1.87(4); C31−P1−Re2 = 113.76(12), C39−P1−Re2 = 111.62(12), C35−P1−Re2 = 110.16(14).

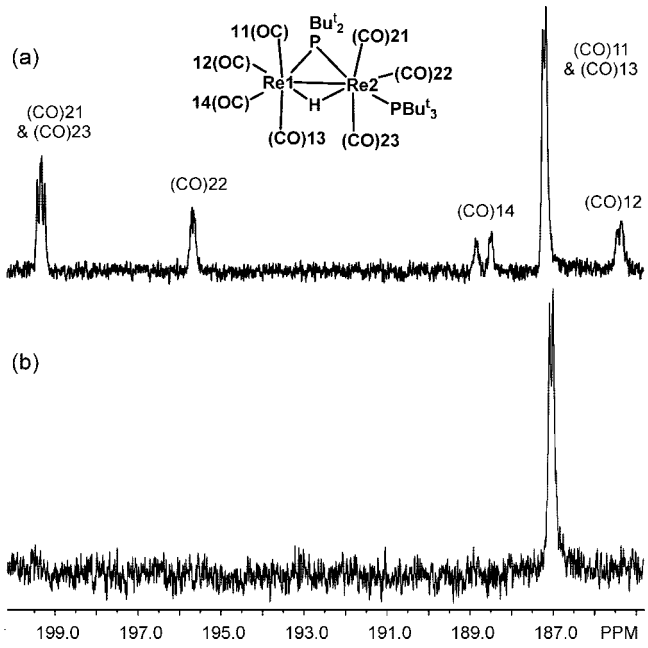

Figure 11. (a) $^{13}C\{^1H\}$ NMR spectrum of **6** having all CO sites enriched to ~30% with ^{13}CO. (b) $^{13}C\{^1H\}$ NMR spectrum of **6** formed by the addition of ^{13}CO to a sample of **4** containing CO at the natural abundance level.

Scheme 3

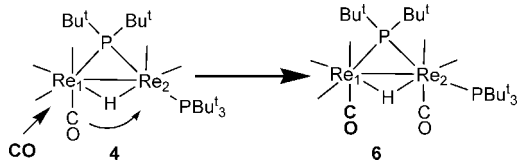

CO(23), lies precisely in the position where the vacant site was located in **4**. Compound **6** thus has 34 valence electrons between the two rhenium atoms, and it is electronically saturated. The Re1−Re2 bond distance has increased in length by 0.07 Å to 3.17813(18) Å on going from **4** to **6**. The *tert*-butyl group in **4** that made the close approach to the vacant site, C(31), has backed away in **6**, and all C−P−Re angles are now greater than 110°, C31−P1−Re2 = 113.76(12)°, C39−P1−Re2 = 111.62(12)°, C35−P1−Re2 = 110.16(14)°. The hydrido ligand H1 was located and refined crystallographically. It has shifted back into the Re1, Re2, P2 plane, and its ^1H NMR resonance has shifted to a higher field value, $\delta = -14.01$ (dd, ^2J(P,H) = 15 Hz, ^2J(P,H) = 8 Hz). The $^{13}C\{^1H\}$ NMR spectrum of **6** (enriched with ^{13}CO to 30%) at room temperature is shown as the top spectrum in Figure 11. There are five resonances. The observed splittings are due to $^{31}P-C$ couplings. A selective phosphorus decoupling $^{13}C\{^1H\}\{^{31}P\}$ NMR experiment revealed that the three resonances at 188.6 ppm (^2J(P2,C) 25.9 Hz), 187.2 ppm (^2J(P2,C) 5.9 Hz), and 185.4 ppm (^2J(P2,C) 6.8 Hz) are coupled only to the bridging phosphorus atom P2, while the two resonances at 199.3 (^2J(P1,C) 8.0 Hz, (^2J(P2,C) 5.5 Hz) and 195.7 ppm (^2J(P1,C) 5.2 Hz, (^2J(P2,C) 3.0 Hz) are coupled both to P1 and to P2. The three resonances coupled only to P2 are assigned to the carbonyl ligands on Re(1). The resonance at 188.6 ppm is assigned to (CO)14 trans to P2 and therefore exhibits the largest P−C coupling of all (^2J(P2,C) 25.9 Hz). The resonance at 187.2 ppm (2C) is assigned to the two equivalent ligands CO(11) and CO(13) on the basis of the larger peak intensity, and the resonance at 185.4 ppm is assigned to CO(12). The two resonances that show coupling to both

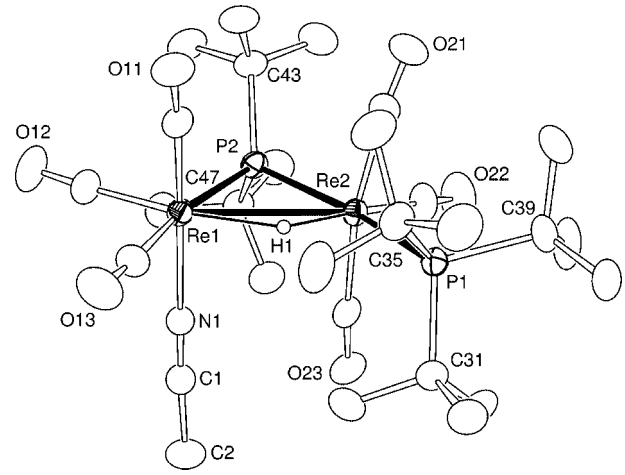

Figure 12. ORTEP of the molecular structure of **7** showing 30% thermal ellipsoid probability. Selected interatomic bond distances (Å) and angles (deg) are as follows: Re1−Re2 = 3.18077(19), Re1−N1 = 2.150(3), Re1−P2 = 2.5035(9), Re1−H1 = 1.93(4), Re2−P2 = 2.4661(9), Re2−P1 = 2.5789(8), Re2−H1 = 1.72(4); N1−Re1−Re2 = 86.92(8).

phosphorus atoms are assigned to the carbonyls on Re2. The two equivalent CO ligands CO(21) and CO(23) are assigned to the resonance at 199.3 ppm because of the relative peak intensity, and the resonance at 195.7 ppm is assigned to CO(22). To identify the site of CO addition, ^{13}CO was added to a sample of **4** having its ^{13}CO level at the natural abundance level. The resulting spectrum is shown in the bottom spectrum of Figure 11. Only one resonance was observed, and it corresponds to the sites (CO)11 and (CO)13. This clearly demonstrates that the added CO ligand was added at the electronically saturated metal atom Re1 and was not directly added to the vacant site on Re2. The CO ligand that occupies the vacant site in **6** must have been one of the originally coordinated CO ligands, and the increase in the number of CO ligands on the phosphine-substituted metal atom Re2 must have been the result of a shift of one of the CO ligands on Re1 to Re2; see Scheme 3.

One can only speculate as to why ligand addition proceeds at the saturated metal atom Re1 and not directly to the unsaturated metal atom Re2, but this might be due to the presence of the bulky PBu$^t_3$ ligand on Re2. As noted above, the methyl group C32 on one of the *tert*-butyl groups does appear to cover the vacant site and could block the direct addition of an uncoordinated molecule to this metal atom. Thus, it might be easier to shift a coordinated CO ligand from the neighboring metal atom Re1 to Re2 and the CO addition could then occur at Re1. The CO shift may precede or more likely accompanies the CO addition to Re1. It is less likely that the shift comes after the CO addition to Re1. When a solution of **6** in heptane solvent was heated to reflux for 1½ h, it was converted back into **4** in 96% yield.

To pursue the study of ligand additions to **4** further, reactions of **4** with MeCN and PhCN were investigated. Both reactions yielded 1:1 adducts with these compounds. The MeCN complex **7** was isolated in 82% yield. The PhCN complex **8** was isolated in 44% yield. The structures of both complexes were established crystallographically, and ORTEP diagrams of the molecular structures of **7** and **8** are shown in Figures 12 and 13, respectively. For both complexes it can be seen that the nitrile was added to the electronically saturated rhenium atom Re1, and there is a CO ligand in the former vacant site on Re2. Thus, as in the CO addition to form **6** from **4**, the addition of nitriles

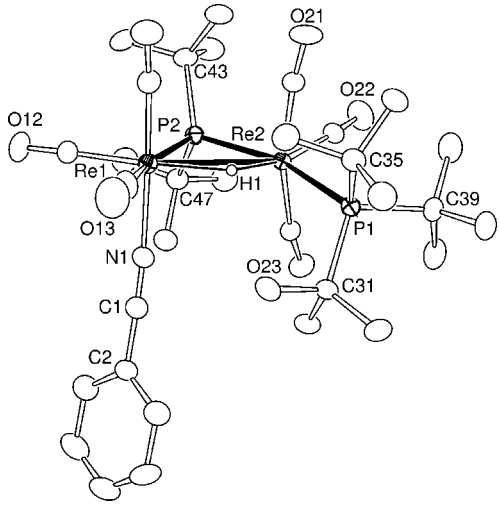

Figure 13. ORTEP of the molecular structure of **8** at 30% thermal ellipsoid probability. Selected interatomic bond distances (Å) and angles (deg) are as follows: Re1−Re2 = 3.1644(2), Re1−N1 = 2.142(3), Re1−P2 = 2.4931(11), Re2−P2 = 2.4596(10), Re2−P1 = 2.5772(10), Re1−H1 = 1.91(5), Re2−H1 = 1.69(5); N1−Re1−Re2 = 91.31(10).

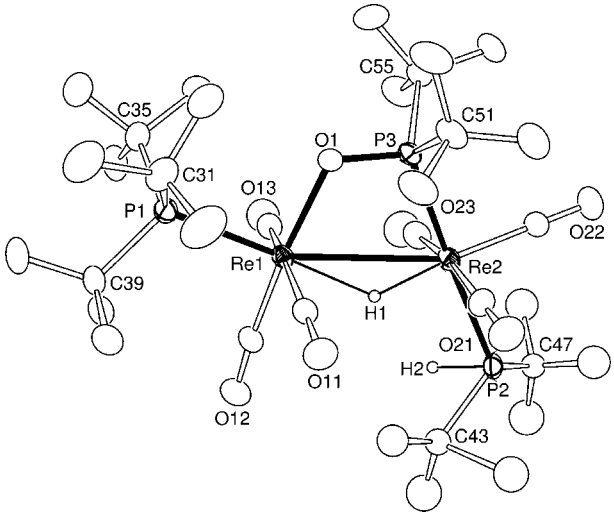

Figure 14. ORTEP showing the molecular structure of **9** at 30% thermal ellipsoid probability. Selected interatomic bond distances (Å) and angles (deg) are as follows: Re1−Re2 = 3.3711(5), Re1−O1 = 2.185(6), Re1−P1 = 2.539(2), Re2−P3 = 2.465(2), Re2−P2 = 2.522(6), P3−O1 = 1.565(6), Re1−H1 = 2.10(9), Re2−H1 = 1.66(9); P3−Re2−P2 = 172.42(15), P2−Re2−Re1 103.92(15), O1−P3−Re2 = 108.7(2), P3−O1−Re1 = 117.1(3).

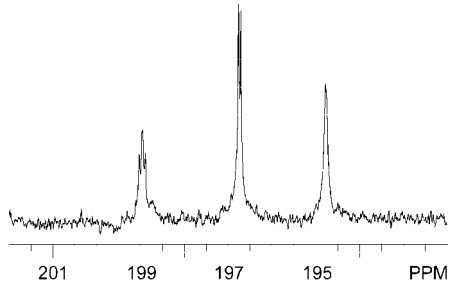

Figure 15. $^{13}C\{^{1}H\}$ NMR spectrum of **9** at room temperature in d_8-toluene solvent.

to **4** also proceeds mechanistically by addition to the electronically saturated, 18-electron rhenium atom Re1 followed by a

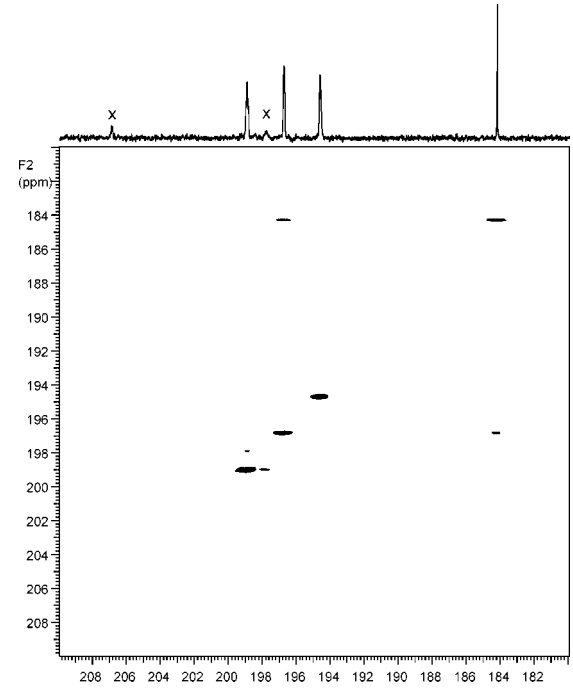

Figure 16. Two-dimensional EXSY (NOESY) $^{13}C\{^{1}H\}$ NMR spectrum of **9** at 60 °C in d_8-toluene solvent in an atmosphere of ^{13}CO. Data were acquired at 125.8 MHz with a 500 ms mixing time. Signals labeled with "x" are from traces of impurity of **5**.

Scheme 4

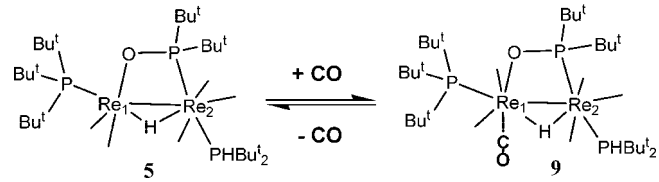

shift of one of the CO ligands to Re2. The Re−Re bond lengths in **7** and **8** are similar to that in **6**, 3.18077(19) and 3.1644(2) Å, respectively. The hydrido ligands were located in both compounds and were found to be bridging ligands across the Re−Re bond in the plane of the Re1, Re2, P2 triangle. This is consistent with the highly shielded resonances observed for these ligands in their ^{1}H NMR spectra: For **7**, $\delta = -11.76$ (dd, $^{2}J(P,H) = 16$ Hz, $^{2}J(P,H) = 9$ Hz) and for **8**, $\delta = -11.60$ (dd, $^{2}J(P,H) = 16$ Hz, $^{2}J(P,H) = 9$ Hz). The nitrile ligands lie trans to a CO ligand on Re1, precisely the same location that the CO ligand was added to **4** to form **6**. When compounds **7** and **8** were dissolved in any solvent that does not contain the corresponding nitrile, they were immediately converted back to **4**. The ^{1}H NMR spectrum of **7** in d_3-MeCN solvent did not show the resonance of the MeCN ligand because it was rapidly exchanged with d_3-MeCN from the solvent. The $^{13}C\{^{1}H\}$ NMR spectrum of **7** was obtained by dissolving a sample of **4** in d_3-MeCN that was partially enriched (30%) with ^{13}CO. There are six resonances of equal intensity for the six inequivalent CO ligands. Just as in the $^{13}C\{^{1}H\}$ NMR spectrum of compound **6**, the three higher field resonances at 193.5, 196.2, and 196.8 ppm are assigned to the CO's on Re1. Large coupling, $^{2}J(P2,C)$ 38.5 Hz, for the resonance at 196.8 is attributed to CO(13), which is trans to the bridging phosphine atom P2. The lower field resonances at 200.1, 201.9, and 203.1 ppm are assigned to the CO's on Re2. The resonances at 201.9 and 203.1 ppm are assigned to either CO(11) or CO(13). It is interesting to note that these two CO ligands were equivalent in compound **6** at 195.7 ppm; however, they are now inequiva-

Scheme 5

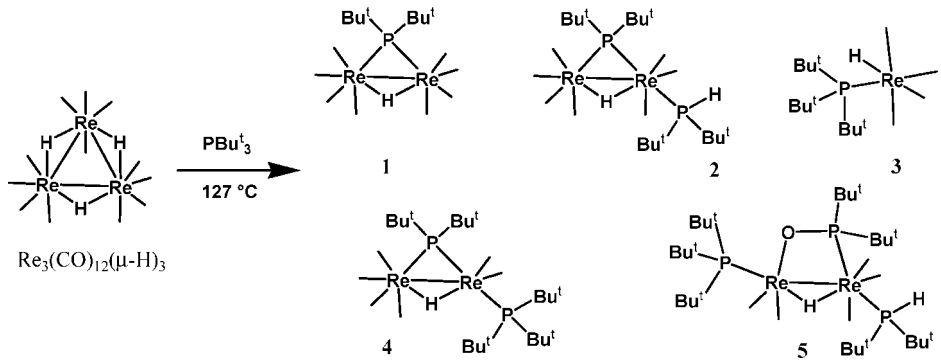

lent due to the lowering of the symmetry produced by the presence of the NCMe ligand.

To investigate the properties of the ligand-deficient complex **5**, it was also treated with CO. The reaction of **5** with CO gas at 25 °C/1 atm appeared to be complete in a matter of minutes, and the product **9** was obtained in 57% yield by cooling the reaction solution to −80 °C overnight, under an atmosphere of CO. Compound **9** is a CO adduct of **5**. It was characterized by a single-crystal X-ray diffraction analysis, and an ORTEP diagram of the molecular structure of **9** is shown in Figure 14. Like **5**, compound **9** is a dirhenium complex that contains a bridging $OPBu^t_2$ ligand and a bridging hydrido ligand across a Re−Re bond. The Re−Re bond is longest of all the compounds that we have reported in this study, Re1−Re2 = 3.3711(5) Å, but there is still a Re−Re single bond present. The longer length of the Re−Re bond in this molecule can be attributed to the presence of two bulky phosphine ligands and one bulky phosphidoxo ligand. The phosphidoxo ligand is a two-atom bridge as in **5** with O1 bonded to Re1 and P3 bonded to Re2, Re1−O1 = 2.185(6) Å, Re2−P3 = 2.465(2) Å. The P−O distance is similar to that in **5**, P3−O1 = 1.565(6) Å. The hydrido ligand was located but refined with a fixed isotropic thermal parameter. In this molecule it lies essentially in the Re1, Re2, P3 plane. Its resonance is very highly shielded, $\delta = -17.95$ and it is coupled to all three phosphorus atoms, ^2J(P1,H) = 17 Hz, ^2J(P2,H) = 8 Hz, ^2J(P3,H) = 5 Hz. Unlike **5**, compound **9** has eight terminally coordinated ligands. Atom Re1 has three CO ligands and one PBu^t_3 ligand, and Re2 has three CO ligands and a PBu^t_2H ligand. Thus, compound **9** is electronically saturated; both metal atoms have 18-electron configurations.

To try to ascertain the site of CO ligand addition to **5** to form **9**, a solution of **9** was placed in an NMR tube under an atmosphere of ^{13}CO at room temperature. The spectrum was recorded as quickly as possible and showed that all CO ligand sites were rapidly and equally enriched with ^{13}CO. This ^{13}C NMR of **9** is shown in Figure 15. It exhibits only three resonances of equal intensity. The resonance at 199.0 ppm appears as a triplet, really as a doublet of doublets, ^2J(P2,C) = 8 Hz, ^2J(P3,C) = 8 Hz), and is assigned to the two equivalent CO ligands, CO(21) and CO(23), on Re2; see Figure 14 for labeling. The resonance at 196.8 ppm is a doublet (^2J(P1,C) = 6 Hz) and is assigned to the two equivalent CO ligands, CO(11) and CO(13), on Re1. There is only one remaining resonance, a singlet at 194.8 ppm. This is assigned to the two CO ligands CO(12) and CO(22). These ligands are inequivalent, so it must be that their resonances are simply accidently shift equivalent. Since there was no observable selectivity in the addition of ^{13}CO to compound **9**, these experiments did not reveal the site of CO addition to **5**. Evidence for the site of CO addition was revealed, however, by recording a 2D EXSY ^{13}C NMR spectrum of **9** at 60 °C in the presence of free ^{13}CO. This spectrum is shown in Figure 16. Most interestingly, cross-peaks were observed between the free CO, observed at 184 ppm, and the doublet resonance of **9** at 196.8 ppm. If the assignment of this resonance is correct, then this indicates that the free CO is exchanging with the CO ligands on Re1 of **9**, and accordingly with Re1 on **5**. This is shown schematically in Scheme 4. Thus, in contrast to the addition of CO to **4**, the addition of CO to **5** occurs at the electron-deficient, 16-electron metal atom, Re1.

Summary and Conclusions

A summary of the products that were obtained from the reaction of $Re_3(CO)_{12}(\mu\text{-}H)_3$ with PBu^t_3 is given in Scheme 5. Some years ago, Liu reported that the reaction of $Re_3(CO)_{12}(\mu\text{-}H)_3$ with PPh_3 gave the tris-PPh_3 product $Re_3(CO)_9(\mu\text{-}PPh_3)_3(\mu\text{-}H)_3$.[23] We did not obtain any evidence for a tris-PBu^t_3 product of $Re_3(CO)_{12}(\mu\text{-}H)_3$ in our studies with the bulky PBu^t_3 ligand. Instead, mono- and dirhenium products were obtained by reactions resulting from fragmentations of the Re_3 cluster of the parent compound. This may be due to the extreme steric crowding effects of the PBu^t_3 ligand. Two of the products, **2** and **5**, contained PBu^t_2H ligands that were evidently formed by degradation of the PBu^t_3 ligand itself. Three of the products, **1**, **2**, and **4**, contained a combination of a bridging PBu^t_2 ligand and a bridging hydrido ligand also formed by a degradation of the PBu^t_3.

It was found that the steric influences of the PBu^t_3 ligands also have profound effects on the coordination chemistry of the dirhenium complexes. In particular, compounds **4** and **5** are both electronically unsaturated 32-electron complexes. Compound **4** has a well-defined vacant coordination site that is partially occupied by one of the methyl groups from a neighboring PBu^t_3 ligand. No vacant site is evident in compound **5**, but both compounds readily add and eliminate CO to form the electronically saturated adducts **6** and **9**. While compound **9** adds CO at the unsaturated metal atom, surprisingly, compound **4** adds CO and the nitriles MeCN and PhCN by an addition at the electronically saturated metal atom, which is accompanied by a shift of one of the CO ligands from the saturated metal atom to the unsaturated metal atom.

Acknowledgment. This research was supported by the Office of Basic Energy Sciences of the U.S. Department of Energy under Grant No. DE-FG02-00ER14980. Dedicated to the memory of F. Albert Cotton.

Supporting Information Available: CIF files for each of the structural analyses are available. This material is available free of charge via the Internet at http://pubs.acs.org.

OM700790C